J Therm Spray Tech (2020) 29:1968–1981
https://doi.org/10.1007/s11666-020-01090-x

PEER REVIEWED

Effect of Coating Thickness on Fatigue Behavior of AISI 1045 Steel with HVOF Thermal Spray and Hard Chrome Electroplating

Vinh Phoi Nguyen[1] · Thien Ngon Dang[1] · Chi Cuong Le[1] · Dung-An Wang[2,3]

Submitted: 15 March 2020 / in revised form: 30 June 2020 / Accepted: 18 August 2020 / Published online: 8 October 2020

Abstract The effects of coating thickness on the fatigue lives of AISI 1045 steel shaft-bending specimens with WC-10%Co-4%Cr high-velocity oxygen fuel (HVOF) coatings and hard chrome electroplated coatings under cyclic loading conditions are investigated. Residual stress distributions of the HVOF-coated layer and the hard chrome-plated layer were measured. During cyclic fatigue testing, cracks are initiated near the interface between the HVOF coating and the steel substrate and propagate through the substrate to cause final fracture based on experimental results. For the specimens with hard chrome-plated coatings, the fatigue crack is initiated near the top of the coating, propagates through the coating, and then grows in the thickness direction of the steel substrate to cause final fracture. As the coating thickness of the HVOF-coated specimens increases, the fatigue strength of the specimens increases, which can be attributed to the fact that the magnitude of the compressive residual stress near the interface between the substrates and the HVOF coatings is higher when the coating thickness gets higher. As for the hard chrome-plated specimens, the fatigue strength is deteriorated when the coating thickness is increased. The microcrack density in the hard chrome coatings increases with the coating thickness and, therefore, may result in the decreased fatigue strength.

✉ Dung-An Wang
daw@dragon.nchu.edu.tw

[1] HCM City University of Technology and Education, Hochiminh City, Vietnam

[2] Graduate Institute of Precision Engineering, National Chung Hsing University, Taichung, Taiwan

[3] Faculty of Mechanical Engineering, Industrial University of Ho Chi Minh City, Ho Chi Minh City, Vietnam

Keywords coating · fatigue · hard chrome · HVOF · residual stress

Introduction

Hard chrome plating can be applied to improve corrosion and abrasion resistance, and it can also be used to build up undersized or worn parts. With the low friction coefficient and high corrosion and wear resistance, chromium plating has been extensively used to improve properties of parts such as shafts, piston rings, engine valve stems, aircraft landing gear, and engine parts. The use of hard chrome plating, however, has been restricted due to negative environmental effects and health hazards. On the other hand, tensile residual stress and microcracks usually exist in parts with hard chrome plating; thereby, the fatigue strength and static load bearing capacity of the parts is reduced. Gawne (Ref 1) described that high tensile residual stress may be found in chromium coatings. They also discussed that the high residual stress generated during electroplating might be the source of the high dislocation densities in the deposited chromium layer. Pina et al. (Ref 2) showed that cracks grew from the surface of the chromium-plated layer to the interface between the plated layer and the substrate by observing the cracks in the cross sections and the surface after removal of successive layers. They also found that the tensile residual stress has a maximum value at the coating surface, then decreases with increasing depth, and finally increases slightly near the interface between the coatings and the substrate. Nascimento et al. (Ref 3) reported that the microcrack density arises as a relief of the tensile residual stress, and the microcrack density increases as the chromium plating thickness increases. Pfeiffer et al. (Ref 4) employed ball-

indentation tests on the surfaces of steel discs with hard chrome coatings to determine the static load bearing capacity. They concluded that the load bearing capacity of the specimens decreases with an increase in crack density of the coatings.

With low oxide dense coatings, good adhesion to substrates, and adjustable compressive stress in coatings, HVOF thermal spraying is a promising replacement for hard chrome plating. Tipton (Ref 5) reported that compressive residual stresses were present on the surface and slightly below the surface of their HVOF WC-17%Co coatings on AISI 403 steel substrates. Nestler et al. (Ref 6) indicated that HVOF spraying has the advantages of wide range of coating materials, higher deposition rates, fewer process steps, compressive residual stress in certain coatings, and less ecological burden over hard chrome plating. Wu et al. (Ref 7) reported that the coating of AISI 1045 steel by HVOF spraying of WC-10Co-4Cr has high hardness, low porosity, homogeneous WC phase distribution, and high bonding strength. HVOF thermal spraying is also advantageous due to its very low temperature deformation and excellent surface properties. Agüero et al. (Ref 8) demonstrated that their AISI 4340 steel specimens with HVOF WCCoCr coating have higher fatigue strengths compared to those with hard chrome plating. They reasoned that the hard chrome-plated coatings contain high density of microcracks, which causes crack initiated near the surface of the chrome coatings. Kutz (Ref 9) reported that HVOF spray coating can result in high bond strength with extremely dense microstructures. Villalobos-Gutiérrez et al. (Ref 10) investigated fatigue behavior of aluminum alloy specimens coated by HVOF spraying of WC-10C0-4Cr. They found that the HVOF coating delivers a tremendous gain in fatigue life compared with the uncoated specimen. Puchi-Cabrera et al. (Ref 11) reported that HVOF spray coatings with WC-10Co-4Cr, WC-17Co, and Co-Mo-Cr alloys have been successfully used to replace hard chrome plating. Azizpour and Nourouzi (Ref 12) deposited WC-12Co coatings on AISI 1045 steel substrates using HVOF thermal spraying. Puchi-Cabrera et al. (Ref 11) reported that HVOF spray coatings may be employed to reach various coating thicknesses. Legg et al. (Ref 13) described that HVOF coatings can be deposited on different composites and alloys to thicknesses greater than 1 mm.

Due to the shot pinning, grit blasting, heating, and quenching process and the mismatch in thermal expansion between the coating and substrate, various residual stress profiles in the HVOF coating and substrate may be developed. Bonding strength at the interface between the coating layer and the substrate and residual stress distribution in the coating and the substrate play important roles in the determination of the durability and fatigue strength of the HVOF-coated parts. Ibrahim and Berndt (Ref 14) described that the residual stress in the HVOF coatings depends on the thermal condition which is a combination of heating, quenching, and cooling of the coating/substrate system. Silva-Junior et al. (Ref 15) reported that compressive residual stress due to shot peening process before coating was the cause of the increase in fatigue strength of WC-13Co-4Cr HVOF-coated 15-5PH stainless steel. Parts coated by HVOF thermal spraying usually have high cohesion strength and compressive residual stress in the coatings. Compressive residual stress in the coatings is beneficial to the bonding and fatigue behavior of the coating/substrate system. X-ray diffraction (XRD) and hole drilling strain gauge methods have been used to measure the residual stress profiles in the HVOF spray coatings. Azizpour and Nourouzi (Ref 12) developed electro-discharge hole drilling method to measure residual stress at the surface of the WC-12Co coating. The results they obtained are in good agreement with that measured by XRD method. In a previous publication of Nguyen et al. (Ref 16), they examined the effects of coating thicknesses of 30 and 60 μm of hard chrome plating and HVOF spraying on the fatigue strength of AISI 1045 steel. Detailed investigation of residual stress profiles in HVOF coatings and hard chrome coating on the AISI 1045 steel was not conducted. The effects of the coating thickness on the residual stress profile in the coatings and fatigue strength of the specimens are investigated in a deeper way in this paper.

Fatigue cracks may be initiated at the components or geometry inhomogeneity in the coatings near the interface between the coating and the substrate of HVOF-coated specimen and propagated into the substrate. Puchi-Cabrera et al. (Ref 11) reported that the inhomogeneity can be pores, alumina particles embedded in the substrate or notches produced during grit blasting process before HVOF spraying. Silva-Junior et al. (Ref 15) concluded that pores and oxide inclusions at the interface between coatings and substrates were the crack initiation sites in the fatigue testing of their HVOF-coated specimens. In hard chrome-plated specimens, cracks may originate at the specimen periphery of the plated layer, then grew through the plated layer, and finally extended into the substrate as shown in Fig. 1b. Ibrahim and Berndt (Ref 14) reported that the fatigue strength of an AISI 4340 substrate with HVOF WC-17Co coating was higher than that of specimens with hard chrome plating and the uncoated specimens. They attributed the fatigue strength improvement to the compressive residual stress in the coatings imparted by the HVOF spray process. Voorwald et al. (Ref 17) reported that deposition of hard chrome plating may cause a decrease in the fatigue strength of the substrate. They also indicated that the high tensile residual stresses in the

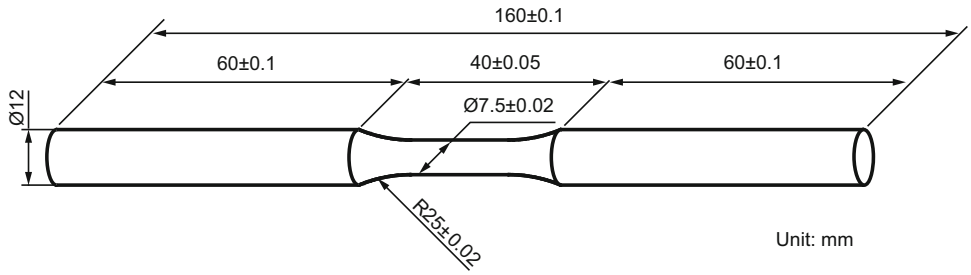

Fig. 1 Dimensions of a rotating bending specimen

chromium coatings may be relieved by local microcracking in the plating process.

The influence of coating thickness on the residual stress distribution and the fatigue behavior of AISI 1045 steel substrates coated with a WC-10Co-4Cr cermet by HVOF thermal spraying is studied in this investigation. Fatigue behavior of the AISI 1045 steel substrates coated by a hard chrome plating is also studied. Microstructures, failure mechanisms, and fatigue lives of the coated systems under rotating bending conditions are investigated based on experimental observations. Scanning electron microscopy (SEM) was used to observe crack initiation sites and crack growth in the specimens. The residual stress of the coated system with various coating thicknesses is measured by an X-ray diffraction method. WC-10Co-4Cr cermet deposited by HVOF thermal spray on various substrates has been extensively studied. The effects of coating thickness on the residual stress distribution and fatigue life of the cermet-coated system are discussed in this investigation.

Experiments

Specimens

Material of the specimens adopted in this investigation is an AISI 1045 steel. Table 1 lists the chemical compositions (wt.%) of the AISI 1045 steel. The hot-rolled steel shows anisotropy in microstructure, texture, and mechanical behavior. For the purpose of removal of the texture and attainment of homogeneous grain distribution, the hot-rolled steel was annealed at 950 °C for 15 min to remove the strong texture and subsequently annealed twice at 840 °C and 760 °C, to attain grain homogeneousness. It was recognized that the selected temperatures were higher than the typical A1 and A3 temperatures of medium-carbon steels. Experiments were carried out to examine the temperatures to remove texture thoroughly. The size of the specimens might demand higher baking temperatures in order to decrease the annealing time. The strong textures of the AISI 1045 rolled steel were removed using the annealing process. The results also showed that the process achieved grain homogeneousness.

Table 1 Chemical compositions (wt.%) of AISI 1045 steel

C	Si	Mn	P	S	Ni	Cr	Cu
0.46	0.21	0.64	0.021	0.007	0.04	0.09	0.16

Table 2 Parameters of the grit blasting process

Blast pressure	4 bar
Working distance	150 mm
Angle between nozzle and blasted surface	75°
Size of blast media Al_2O_3	0.443–0.686 mm

Mechanical properties of the AISI 1045 material were obtained in accordance with the tensile testing standard ISO 6892–1: 2009. The tensile and yield strength of the AISI material are 1083 and 1143 MPa, respectively. The averaged values of the tensile and yield strength are 1143 and 1083 MPa, respectively. The tensile strength of the AISI 1045 steel subjected to quenching and tempering can be higher than the typical tensile strength of AISI 1045 steels of 570–700 MPa after hot rolling. The tensile strength of AISI 1045 after quenching and tempering can be higher than 1000 MPa. Specimens for rotating bending fatigue tests were machined from the material by a CNC lathe, according to ISO 1143: 2010. Dimensions of the machined specimens are schematically shown in Fig. 1. Growth of martensite microstructure and residual stress relief of the specimens were achieved by quenching at 840°C in water and tempering at 600°C for 30 min, respectively. Grit blasting was adopted to acquire desired surface roughness of the specimens. Greater adhesion between the coating layer and the substrate can be attained by appropriate surface roughness through better mechanical interlocking at their interface. The values of the parameters for the grit blasting process are listed in Table 2. The surface roughness of the specimen after the grit blasting is nearly $\sim$ 4.3 μm Ra.

HVOF spray coating was carried out using a Jet Kote HVOF spray system (Stellite Coatings, Inc., USA). Table 3 lists the values of HVOF spray parameters. The liquefied

Table 3 Parameters for HVOF spray coating

Oxygen pressure	150 lb/in^2
Oxygen flow rate	200 L/minute
Liquefied petroleum gas pressure	50 lb/in^2
Fuel flow rate	40 L/minute
Air pressure for powder feeder	90 lb/in^2
Carrier gas flow rate	10 L/minute
Spray distance	210 mm
Rotary speed	240 rpm
Impingement angle	85°
Traverse speed	600 mm/minute

petroleum gas includes 50% propane (C_3H_8) and 50% butane (C_4H_{10}). The processing parameters were provided by the manufacturer for producing a dense coating. The WC-10Co-4Cr powder (WOKA 3652, Oerlikon Metco Co. Ltd., Switzerland) has a particle size ranging from 15 to 45 µm. The thickness of the coated layer was measured using a thin film thickness gauge (MiniTest 600B, Elektrophysik, Germany). Hard chrome electroplating on the same substrates was carried out in order to compare the effects of thickness on fatigue strength and residual stress with the HVOF spray coating. A plating solution with a chromic acid solution containing chromic acid in a concentration of 250 g/L was used in the hard chrome electroplating. Sulfuric acid in a concentration of about 2.5 g/L of solution was added as a catalyst. A current density of 40 A/dm^2 was applied. The deposition rate was in the range of 30 µm/h at 55°C. The averaged value of the surface roughness of the hard chrome electroplated layer of randomly selected three specimens was 0.77 µm Ra.

Determination of Residual Stress in the Surface Layer of Coating

Residual stress at various depths of the coated layers on the substrate of the specimens was measured by an XRD technique following the procedures reported by Le (Ref 18). The lattice strain was evaluated from the comparison of the lattice spacing of an *(hkl)* diffraction peak with that of a stress-free specimen. The elastic lattice strain was then used to calculate the stresses through the Hooke's law. Cu-Kα radiation with a wavelength λ of 1.54056 Å was used for the diffraction measurements through an X-ray diffractometer (X'Pert Pro, Malvern Panalytical Ltd., UK). The residual stress at various depths of the coatings of the specimens was measured following the removal of coating layers by grinding and etching for HVOF-coated layers and hard chrome electroplated layers, respectively. The HVOF-coated layers were ground with a diamond wheel; then, a 5–7 micron diamond paste was adopted to reach the required depth, following the low stress grinding process described in Azizpour and Nourouzi (Ref 12). Azizpour and Majd (Ref 19) evaluated the residual stress profile of HVOF WC–Co coatings on AISI 1045 steel by means of XRD after removing surface layers by mechanical grinding. The XRD using the Cu-Kα radiation has a penetration depth of about 2–5 µm. Therefore, the background scatter of the substrates should have a minimal effect on the diffraction lines of the coated layers. In this investigation, the focus is on the effects of the coating thickness on the fatigue strength of AISI 1045 steel with HVOF spray coating. The residual stress in the HVOF-coated layers is considered to be an important factor to influence the fatigue strength of the tested specimens. The general trend of the residual stress distribution in the coating layers with various thicknesses is more concerned than the residual stress values. The chrome electroplated coatings were removed by etching in a hydrochloric acid solution. The etching process of the chrome-plated surface layers is similar to that reported by Eigenmann et al. (Ref 20).

The stresses were evaluated by the $\sin^2\psi$ method as reported in Le (Ref 18). Due to the fact that WC-10Co-4Cr is a multiphase cementite, where tungsten carbide (WC) is the domain phase of the HVOF coatings, the values of the residual stress of the coatings were calculated from the WC diffraction with the measuring 2θ ranging from 82° to 86° for {201} plane diffraction. The residual stresses of hard chrome-plated layers were computed by these 2θ angles for {211} plane diffraction of chromium. The values of the Young's modulus and Poisson ratio of the WC-10Co-4Cr coatings were taken as 316 GPa and 0.22, respectively. Masoumi et al. (Ref 21) calculated the value of the Young's modulus for their WC-10Co-4Cr coating samples. The Poisson ratio and Young's modulus of the hard chrome electroplated layer on the AISI steel were taken as 0.23 and 271 GPa, respectively. Eigenmann et al. (Ref 20) adopted these Young's modulus and Poisson ratio values for their hard chrome coatings on AISI 1045 steel specimens for determination of residual stress in the coatings. Effects of the texture on the elastic and plastic anisotropy of the coatings were not considered in the calculation of the residual stress in the coatings.

Fatigue Test

A four-point bending fatigue testing machine was developed and fabricated for investigation of the fatigue behaviors of the specimens. Figure 2 shows a photograph of the machine. Rotating bending specimens were fixed between four clamps. Two outer clamps constrain the vertical movement of the specimen. The vertical sinusoidal force applied by the two inner clamps facilitates the desired

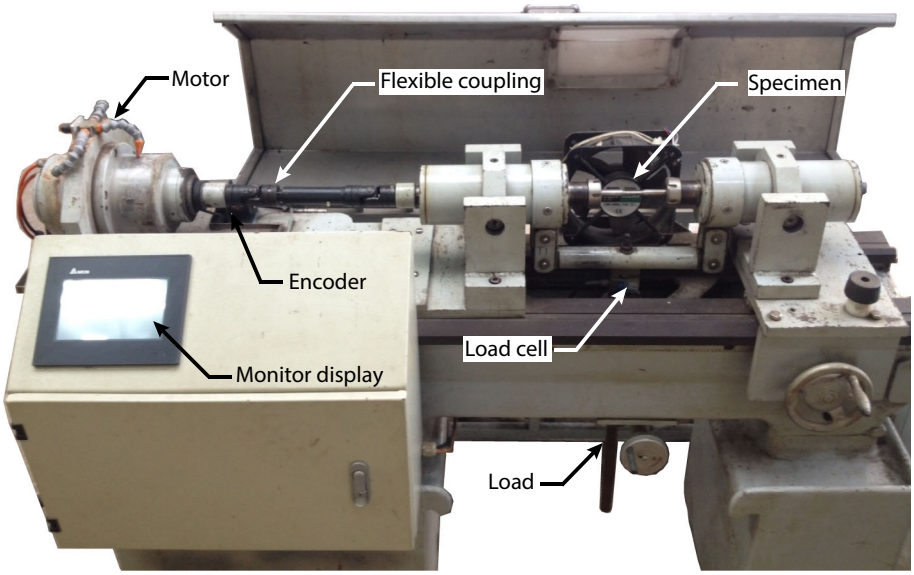

Fig. 2 Photograph of a four-point bending fatigue testing machine

bending of the specimen. Fatigue tests were performed in a controlled force mode. The applied force was measured by a load cell. The number of cycles to failure was recorded by an encoder near the motor spindle. Fatigue tests were carried out under rotating bending conditions with a stress ratio R of -1 and a loading frequency of 50 Hz. The fatigue strength is determined when specimen fracture occurs or the number of cycles reaches 10^7. Fracture of specimens is defined as the increase in vibration amplitude above a preset level.

Results and Discussion

Figure 3(a) shows the microstructure of the hot-rolled AISI 1045 steel with texture and anisotropy. Elongation of the grains along the rolling direction of the steel is observed. Figure 3(b) shows that the texture was removed to attain grain homogeneity after annealing. The grain size of the material ranges from 10 to 20 μm. Figure 3(c) and (d) shows the fine grain microstructures after quenching and tempering, respectively. Platelike or lath-like grains of the as-quenched martensite are shown in Fig. 3(c). The plate microstructure is coarsened after tempering as shown in Fig. 3(d). Some spherodized cementite particles may appear, and the ferrite may have recrystallized into equiaxed grains after tempering. Specimens for fatigue tests were machined from the material from the tempered steel. These specimens were finally ground and polished. Figure 4(a) shows a photograph of a specimen. The specimen was ground and polished, but not grit-blasted. The averaged hardness and roughness of three as-polished specimens are 57.6 ± 1.4 HRC and 0.85 ± 0.02 μm, respectively. The averaged hardness of three specimens after heat treatment is 30.9 ± 0.8 HRC. The hardness value after heat treatment is significantly lower than that of the as-polished specimens. Figure 4(b) and (c) shows a hard chrome-plated specimen and a HVOF WC-10Co-4Cr-coated specimen, respectively. The surface of the hard chrome-plated specimens has a hardness of nearly 64.0 ± 1.2 HRC and a roughness of nearly 0.78 ± 0.04 μm based on measurements of three specimens. The hardness and roughness at the surface of the HVOF-coated specimens are nearly 71.0 ± 7.8 HRC and 6.43 ± 0.09 μm, respectively. The hardness and roughness values were measured at one point on each specimen.

XRD image analyses were examined to reveal crystalline structure phases of the coatings. Figure 5(a) and (b) shows the XRD patterns of the hard chrome coating and the WC-10Co-4Cr coating, respectively. Figure 5(a) shows that the XRD pattern of the electroplated hard chrome coating corresponds to the presence of chrome. As shown in Fig. 5(b), WC constitutes the main phases of the WC-10Co-4Cr coating. Azizpour et al. (Ref 22) described that other phases of W-Co-Cr may exist in the WC-10Co-4Cr coatings. Due to the low content or high dispersion of the phases in the coating, they may not be detected by the XRD analyses.

Residual Stress Measurements

The WC particles in the WC-10Co-4Cr powder used for HVOF coatings were very hard and did not melt under the HVOF spray coating temperature. Compressive stress and plastic deformation in the coatings can be caused by impingement of the hard particles on the steel substrate and previous coating layers at high speed. The cooling process may also induce compressive stress in the coating layer due

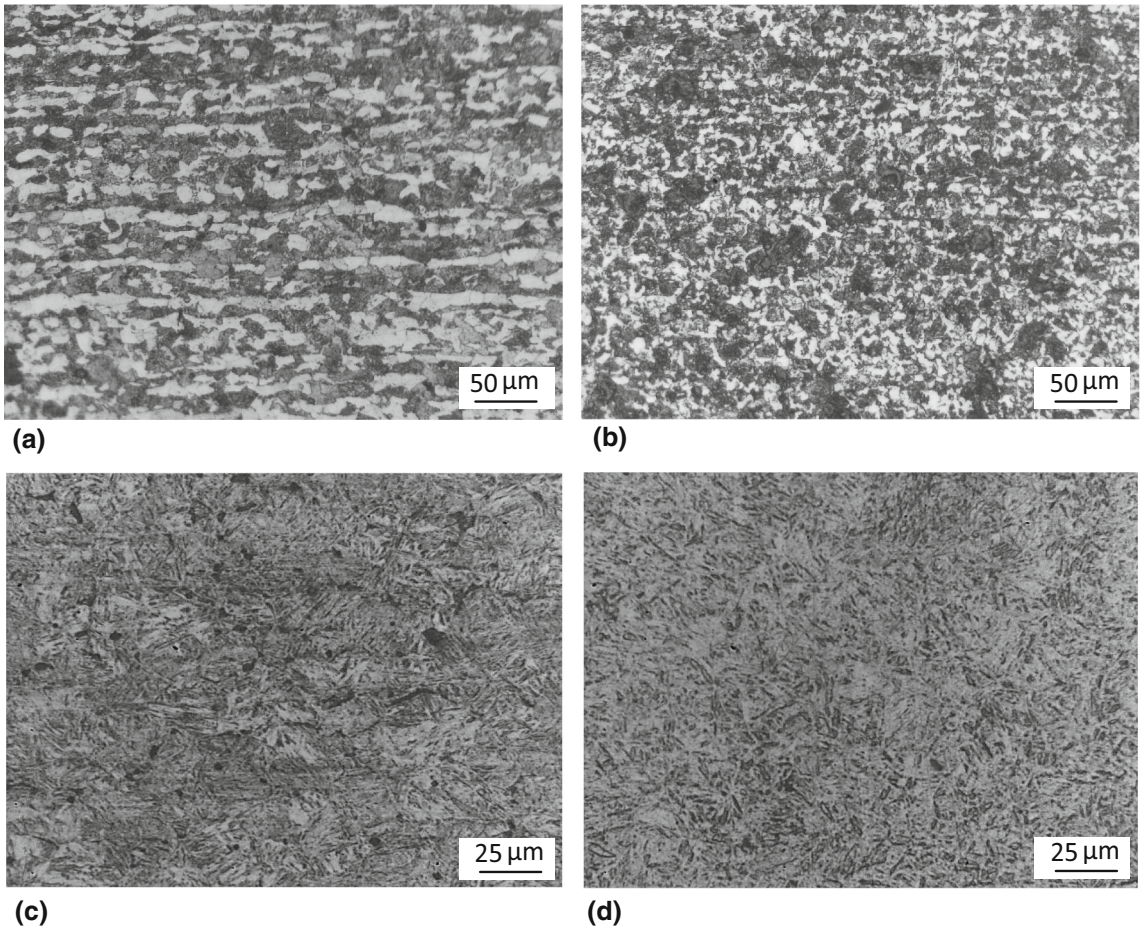

Fig. 3 Microstructures of AISI 1045 steel after (a) hot rolling, (b) annealing, (c) quenching, and (d) tempering

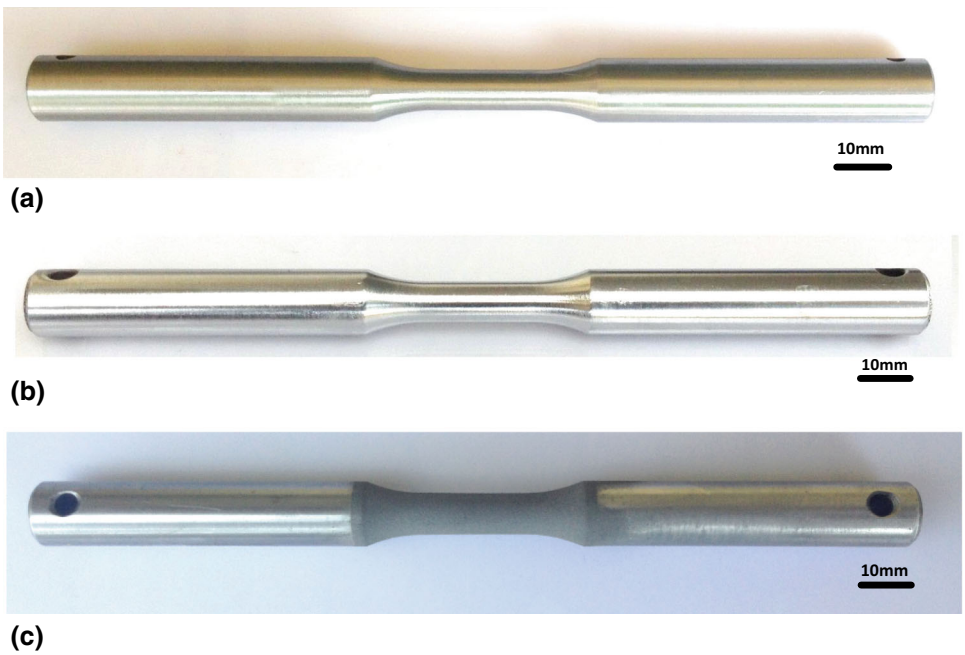

Fig. 4 Photographs of (a) an uncoated specimen, (b) a hard chrome-plated specimen, and (c) a HVOF WC-10Co-4Cr-coated specimen

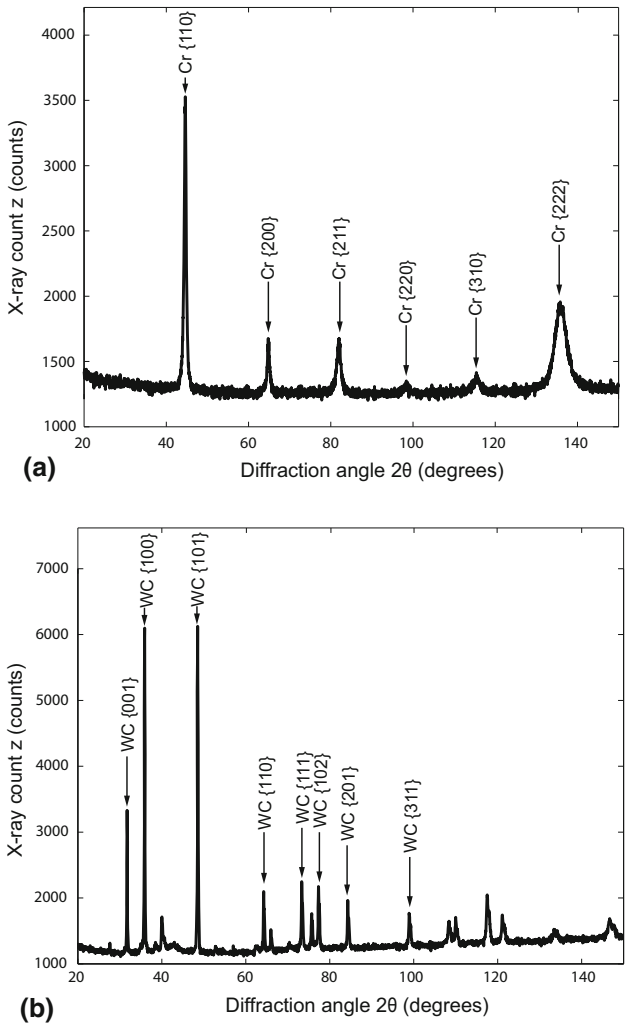

Fig. 5 XRD patterns of (a) hard chrome coating, (b) WC-10Co-4Cr coating

to the fact that the coefficient of thermal expansion of the coating layer is smaller than that of the substrate. The typical values of the coefficient of thermal expansion of AISI 1045 steel and WC-10Co-4Cr coating are $12 \times 10^{-6}\ K^{-1}$ and $5.5 \times 10^{-6}\ K^{-1}$, respectively. Masoumi et al. (Ref 21) reported these values for WC-10Co-4Cr coatings on low-carbon steel samples. Figure 6(a), (b) and (c) shows the SEM photographs of the surfaces of the WC-10Co-4Cr layer with a coating thickness of 31 μm, 63 μm, and 92 μm, respectively. No cracks were observed on the surfaces of those coating layers with various coating thicknesses. Compressive stress may exist in the WC-10Co-4Cr layer.

Figure 6(d), (e) and (f) shows the SEM photographs of the surfaces of the chrome plating layer with a coating thickness of 30 μm, 61 μm, and 93 μm, respectively. A large number of surface cracks were found on those surfaces. The SEM images of the surfaces suggested that these cracks appeared to have been produced by splitting of the surface layers in tension. Tensile residual stress appeared to exist in chrome plating layers. Hydrogen atoms may exist in chrome crystalline lattice in the plating process. Tensile residual stress could be resulted due to the exhaustion of the hydrogen atoms when the plating process was ended. When the tensile residual stress exceeded the cohesive strength of chrome, cracks were induced. Voorwald et al. (Ref 23) reported that tensile residual stress in hard chrome plating is caused by chromium hydrides decomposition during plating. Ibrahim and Berndt (Ref 14) found that the decomposition is accompanied by volume shrinkage and crack formation.

The ultrasonic velocities of particles in HVOF thermal spraying process can produce compressive residual stresses in the coating layers. Figure 7 shows the through-thickness residual stress distributions of HVOF WC-10Co-4Cr coatings with coating layer thicknesses of 31, 46, 63, 77, and 92μm. The penetration depth of the Cu-Kα radiation of the XRD is about 2−5μm. The residual stress was actually measured at a distance 2−5μm smaller than the marked distance in the figure. Each coating exhibits a compressive stress, and the stress remains compressive at the interface between the coating and the substrate. Magnitudes of the compressive residual stress increase as the distance from the substrate decreases for the five cases. The residual stress at the interface is also shown in an inlet of Fig. 7. The compressive stress magnitude at the interface increases from 609 to 735 MPa as the coating thickness increases from 31 to 92 μm. Lyphout et al. (Ref 24) reported that quenching and peening stresses are the major stress components in HVOF coatings, and the high-speed, semi-molten particles can cause large peening stress. The high particle speed may cause a local compressive stress in the substrate and the deposited coating layer. Valarezo et al. (Ref 25) described that tensile residual stress in the coatings of HVOF spraying due to solidification and contraction during cooling can be relieved via inelastic mechanisms such as yielding, microcracking, or creep, and the stress state of the coatings changes as a result of plastic deformation and peening effect from the incoming particles, which imposed compressive stress in the already deposited layers. Kuroda et al. (Ref 26) reported that the kinetic energy of sprayed particles of the HVOF spraying plastically deforms the surface layer of the target and induces a significant level of compressive stress. Sampath et al. (Ref 27) presented that high velocity impact of HVOF spraying caused plastic deformation of the surface layer and generated compressive stress (peening stress). Bansal et al. (Ref 28) reported that significant peening stresses were generated during impact of molten and semi-molten particles on the substrate during an HVOF spraying process. Gui et al. (Ref 29) described that the impingement of HVOF spraying will cause plastic deformation on the

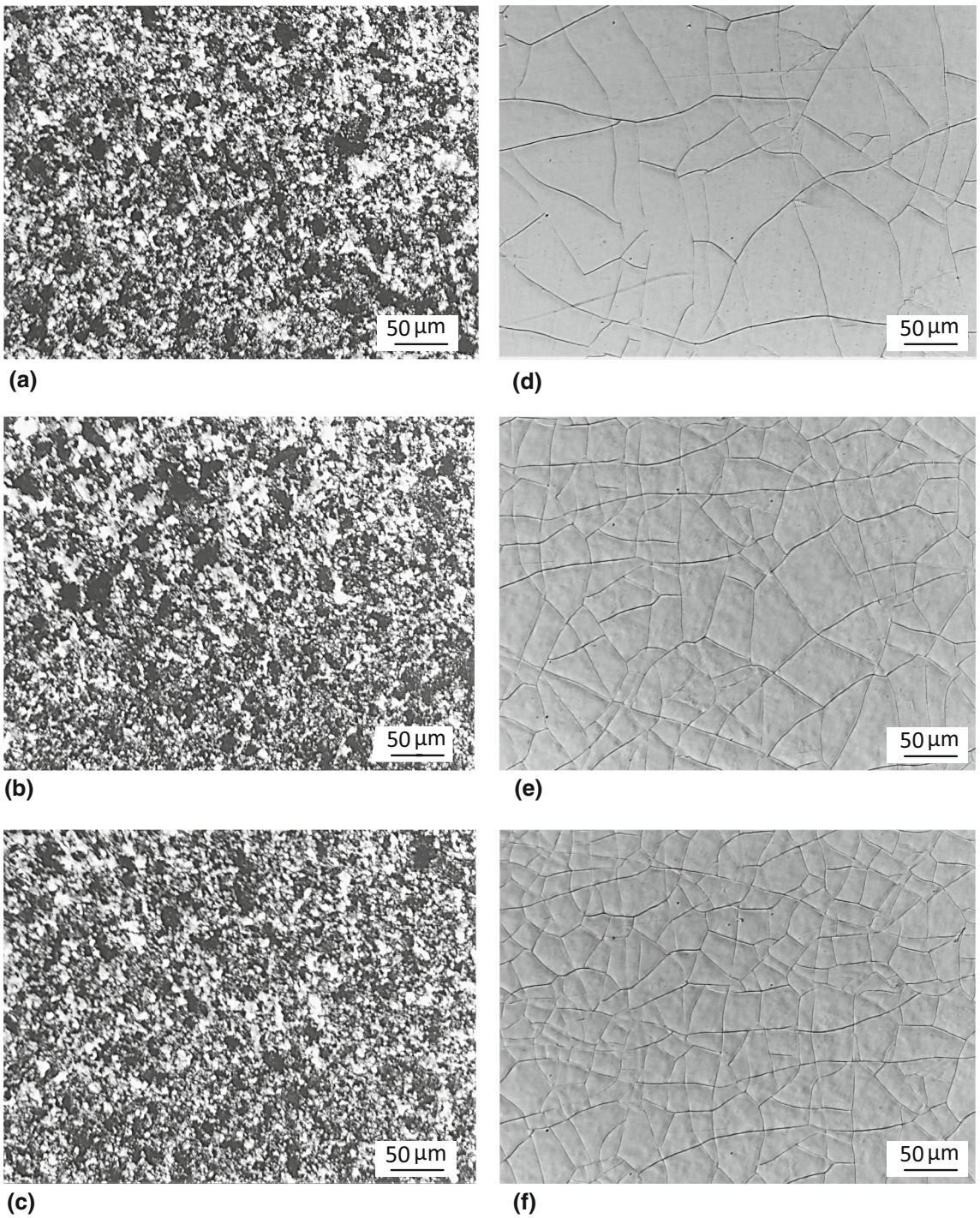

Fig. 6 SEM photographs of coating surfaces. WC-10Co-4Cr layer with a coating thickness of 30 µm (a), 60 µm (b), and 90 µm (c). Hard chrome layer with a coating thickness of 30 µm (d), 60 µm (e), and 90 µm (f)

preexisting material surface, and a compressive residual stress will be induced in the coating.

Residual stress at the bottom of coating layers is actually the residual stress at the surface of the substrates after coating layer was fully removed. The grit-blasting created high compressive stress at the surface of the substrates. As the coating thickness increases, the distance between the nozzle outlet and the surface of the specimens is decreased. Therefore, the kinetic energy of particles of the spray increases the compressive stress in the coated layers and contributes to the slight increase in the compressive stress at the surface of the substrates.

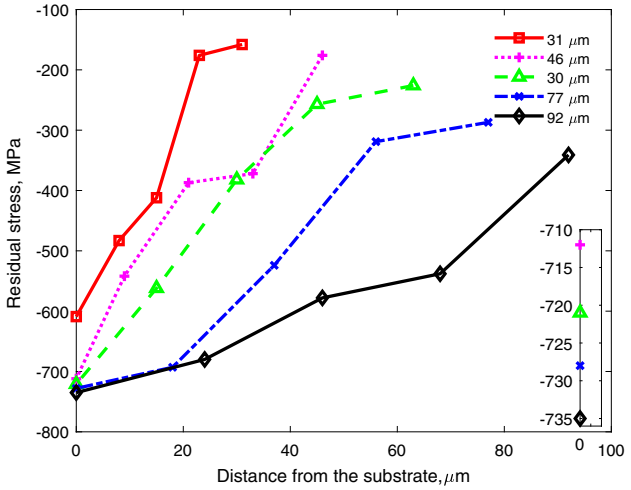

Fig. 7 Residual stress distribution along the thickness direction of HVOF coatings with various coating layer thicknesses

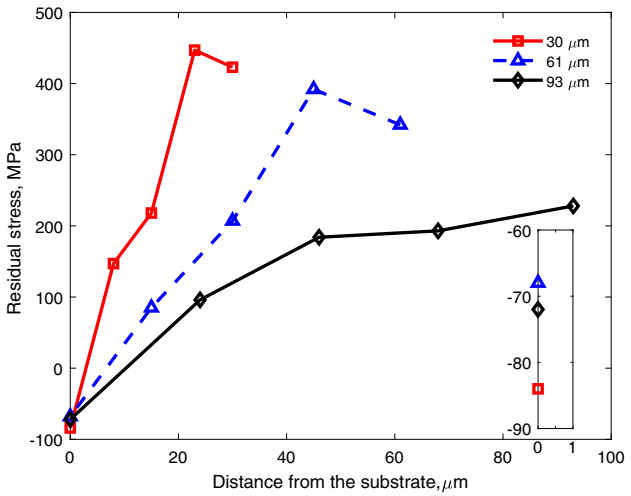

Fig. 8 Residual stress distribution along the thickness direction of hard chrome coatings with various coating layer thicknesses

Figure 8 shows the through-thickness residual stress distributions of hard chrome coatings with coating layer thicknesses of 30 µm, 61 µm, and 93 µm. The residual stress values at the top surface of the electroplated coatings, from 423 to 228 MPa, decrease with increasing thickness of the layers, from 30 to 93 µm. Ohtsuka et al. (Ref 30) observed a similar trend. The residual stress profiles show a decreasing trend toward the interface between the coatings and the substrate. The residual stress is tensile throughout the depth of the coatings except near the interface. Nascimento et al. (Ref 3) described that tensile residual stress in electroplated chromium coatings decreases with the depth of coating. Pina et al. (Ref 2) reported that tensile residual stresses in hard chrome coatings is due to the inclusion of oxygen and hydrogen co-deposited with chromium. The tensile residual stress was generated by the inclusion of those elements in the crystallographic lattice and in solid solution. The compressive residual stresses at the interfaces for the three cases fall in the 76 ± 10 MPa interval, and may be taken as unaffected by the coating thickness. Pina et al. (Ref 2) discussed that the compressive stress at the interface can be related to the grit-blasting for the substrates. Pina et al. (Ref 2) also showed that as the coating thickness is increased, the averaged values of the tensile residual stress is decreased, and the residual stresses in the coatings tended to stabilize at a certain value near the interface.

Fatigue Testing

Figure 9(a) and (b) shows the photographs of a failed HVOF spray-coated specimen and a failed hard chrome-plated specimen during the rotating bending fatigue tests with stress amplitudes of 475 MPa and 420 MPa, respectively. Close-up views near the fractured portion of the specimens are shown in the inlets. The fractured position are close to the middle of the reduced section of the specimens. Figure 10(a) shows a SEM photograph of the fracture surface of a HVOF spray-coated specimen. Several cracks leading to fracture of the specimen are shown in the figure. Figure 10(b) shows a close-up view near the crack. A main crack and a kinked crack are indicated in the figure. The main crack appears to emanate from the interface between the coating and the substrate, and propagates along the interface. The kinked crack is then initiated from the main crack tip at the interface and grows through the substrate. It is perceived that the compressive residual stress in the HVOF coatings retards the nucleation of fatigue cracks in the coating layer. Puchi-Cabrera et al. (Ref 11) reported that fatigue cracks of HVOF coatings can form at the interface between a substrate and its coating near a sharp notch, which can be due to the previous grit blasting process.

Figure 11(a) shows the fracture surface of a chrome-plated specimen. Multiple fatigue cracks were found to propagate toward the center of the specimen. Figure 11(b) shows a close-up view near a crack. The fatigue crack is initiated near the surface of the coating layer, then propagates through the coating, and finally grows in the substrate to cause final fracture. Due to the fact that hard chrome-plated coatings exhibit tensile residual stresses, fatigue crack can nucleate and grow wherein, then through the substrate, and lead to fracture of the specimen. Figure 12(a) shows a zoom in the photograph of the cross section of the coating layer in a failed HVOF-coated specimen. No microcracks were found in the photograph. A zoom in SEM photograph of the cross section of the coating layer in a failed hard chrome-plated specimen is

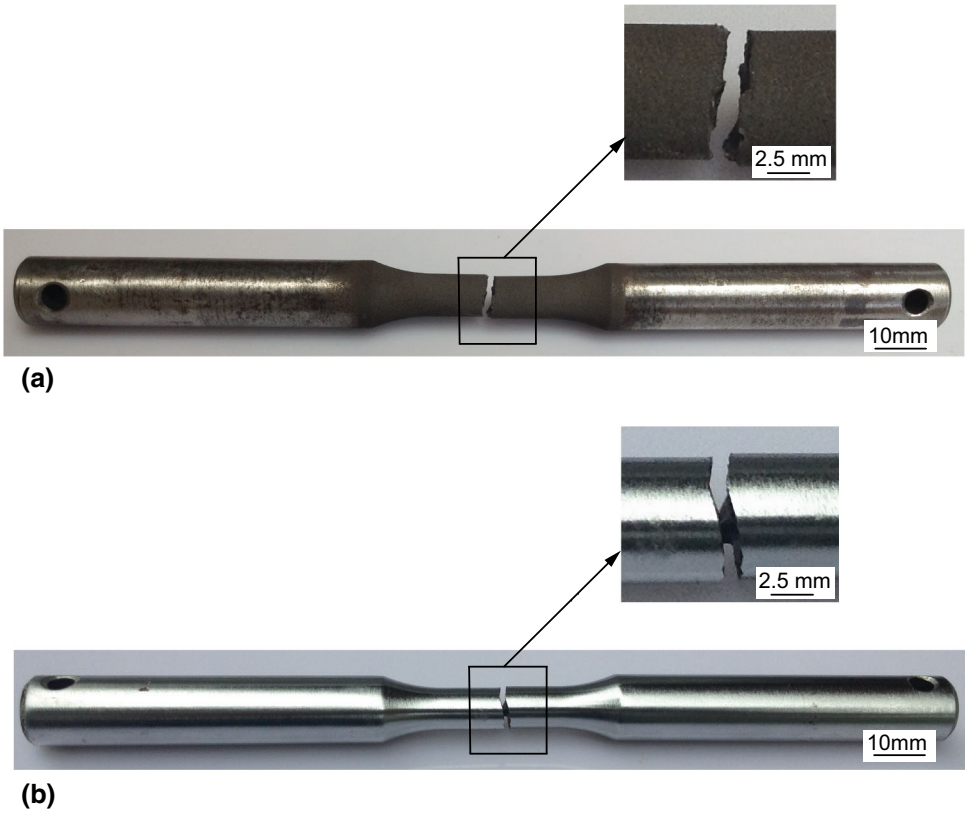

Fig. 9 (a) A failed HVOF spray-coated specimen, and (b) a failed hard chrome-plated specimen

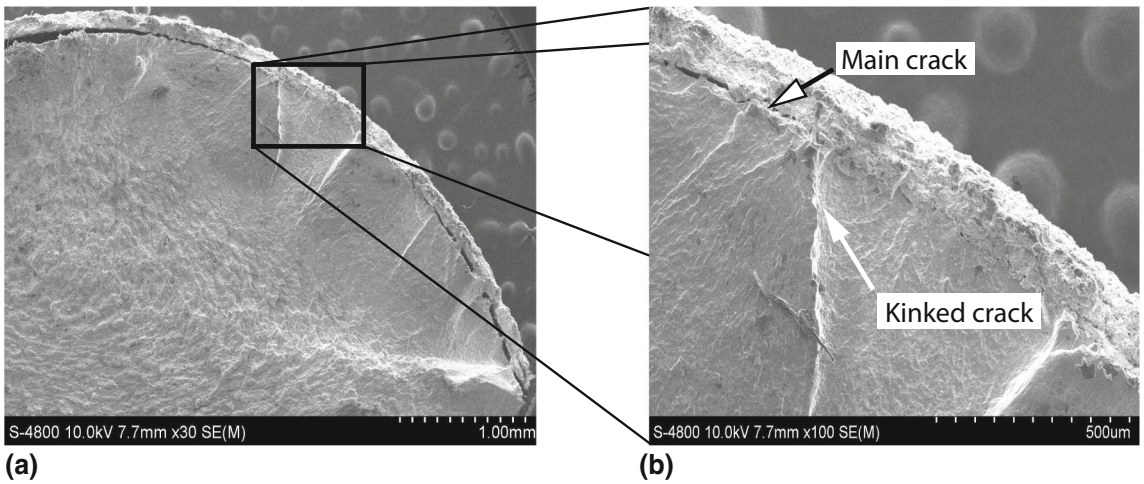

Fig. 10 Micrograph of the fractured surface of a failed HVOF-coated specimen (a), and a close-up view near the fatigue crack (b)

shown in Fig. 12(b), in which a crack has a zigzag path and gradually grows in the coating.

Paths of fatigue crack growth of a HVOF spray-coated specimen and a hard chrome-plated specimen are schematically represented in Fig. 13(a and (b), respectively. As evidenced in Fig. 12, the delamination of the coating from the substrate can be taken as the main crack which propagates along the interface between the coating and the substrate. The fatigue crack propagated at the interface at an early stage. The specimen exhibited good cohesion in the coatings, but poor adhesion at the interface between the coating and the substrate. After the main crack traversed a certain distance, a kinked crack may develop at certain point and lead to fracture of the coated specimen. Costa et al. (Ref 31) observed a fatigue fracture surface of a WC-10%Co-4%Cr thermal spray-coated specimen and reported that cracks grow at the coating/substrate interface under the influence of compressive residual stresses. When the coating layer is relatively harder than the substrate, fatigue crack may propagate into the substrate (Ref 32).

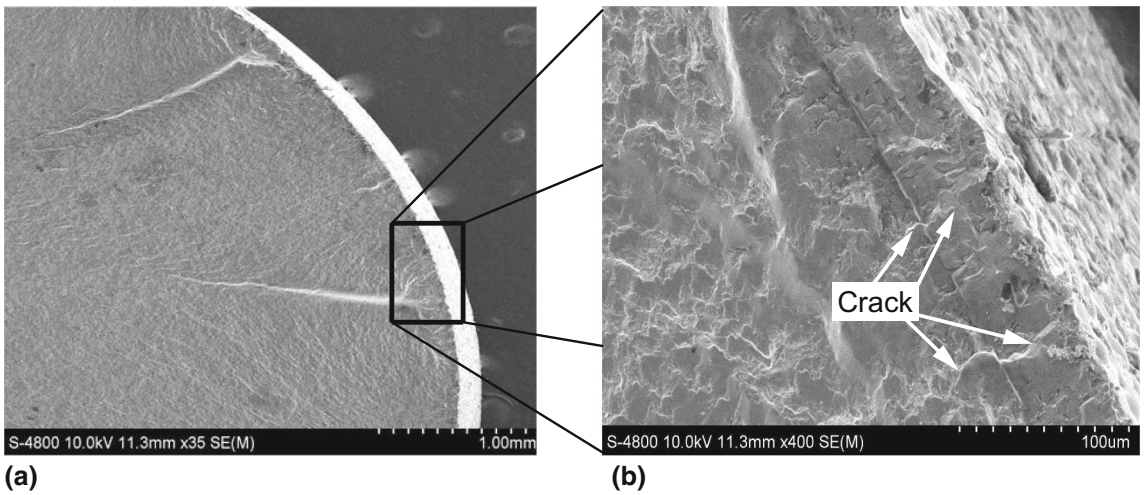

Fig. 11 Micrograph of the fractured surface of a failed hard chrome-coated specimen (a), and a close-up view near the fatigue crack (b)

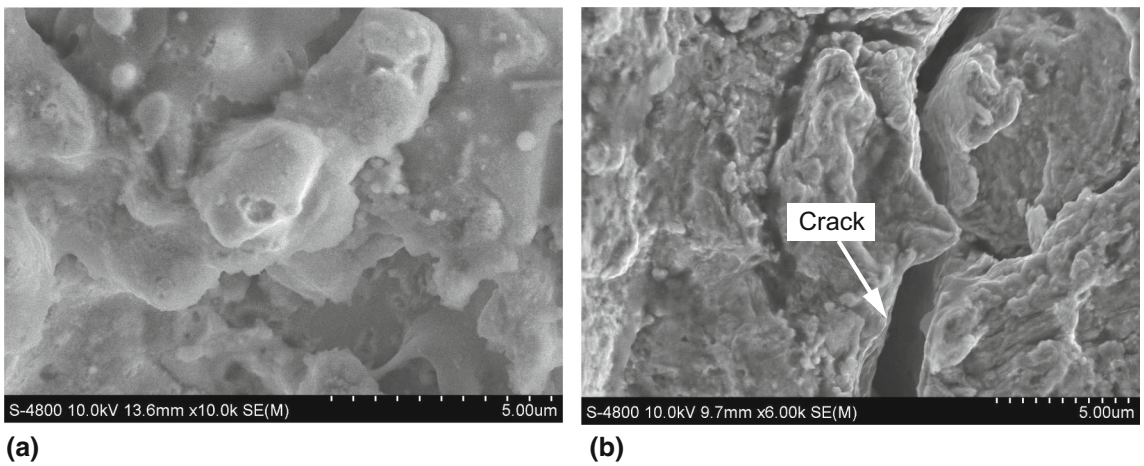

Fig. 12 SEM photographs of cross sections of the coating layers in a failed HVOF-coated specimen (a), and a failed hard chrome-plated specimen (b)

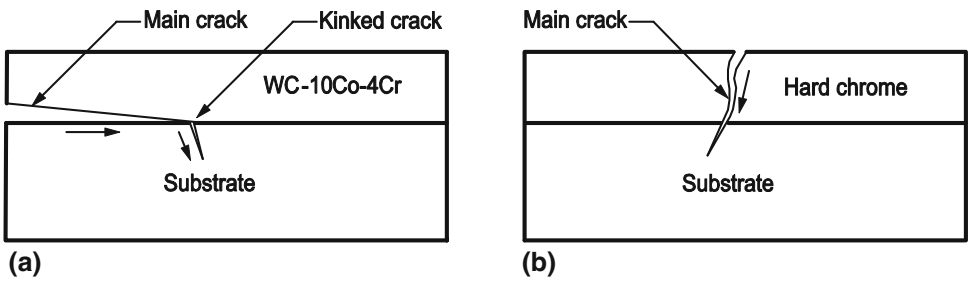

Fig. 13 Schematic of crack growth of specimens coated by (a) HVOF spraying and (b) hard chrome electroplating

The results shown in Fig. 11 for a failed chrome-plated specimen suggest a failure mode of through-thickness crack growth in the coating and crack penetration into the substrate as indicated in Fig. 13(b). A close examination of Fig. 11(b) reveals that the fatigue cracks may originate at the surface of the coated layer. When the tensile residual stress exceeded the cohesive strength of chrome, microcracks were induced. Under the repetitive tension loads, the microcracks may grow and join together to form a main crack and propagate through the thickness of the coatings. It should be noted that the two failure modes, as indicated in Fig. 13(a) and (b), may not be process dependent but be determined by the relationship between the mechanical properties of the coating layer and the adhesion strength.

Figure 14 shows the stress amplitude as a function of the number of cycles to failure of HVOF spray-coated

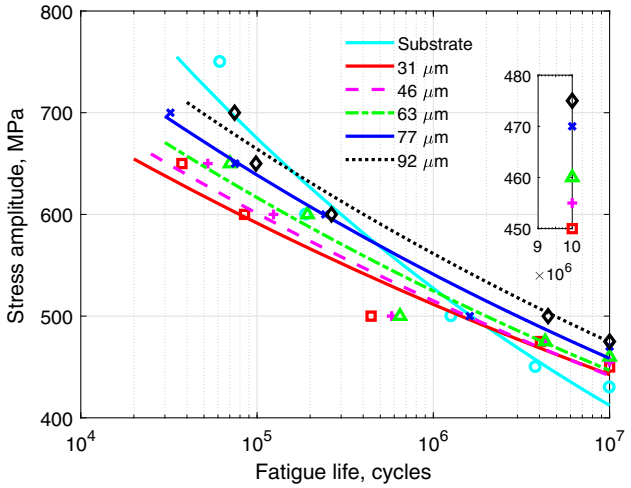

Fig. 14 The stress amplitude as a function of the life of HVOF spray-coated specimens

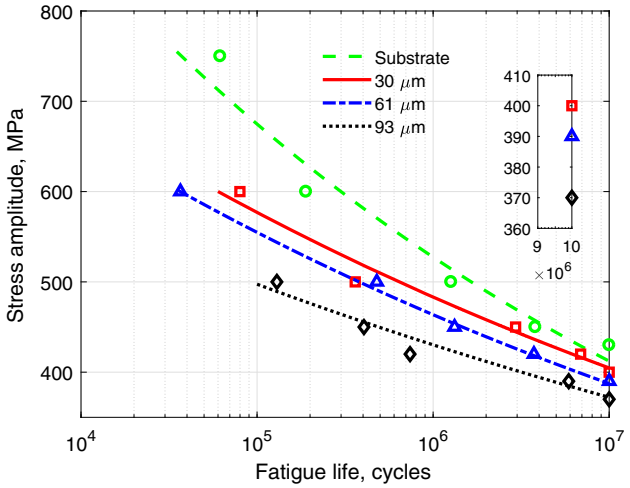

Fig. 15 The stress amplitude as a function of the life of hard chrome-plated specimens

specimens with coating layer thicknesses of 31μm, 46μm, 63μm, 77μm, and 92μm in the rotating bending fatigue tests. The values were averaged from three tests. The stress amplitudes were calculated using the substrate diameter of the specimens. A power law relationship based on the Basquin's equation is used to fit the fatigue curves in the figure. The Basquin's equation can be expressed as (Ref 33)

$$\Delta\sigma = \alpha(N_f)^{\beta} \quad \text{(Eq 1)}$$

where $\Delta\sigma$ is the stress amplitude, α and β are the fitting parameters, and N_f is the number of cycles at failure. An inlet zooming the portion of the figure near the fatigue strength of $N_f = 10^7$ cycles is also shown in the figure. It appears that the fatigue strength increases as the coating thickness increases. As seen in the figure, the fatigue strength of HVOF coatings is generally higher than that of the substrate. The fatigue strength for the specimens coating layer thicknesses of 31, 46, 63, 77, and 92μm is 450, 455, 460, 470, and 475 MPa, respectively. As shown in Fig. 8, the magnitude of the induced compressive residual stress at the interface increases when the coating thickness is increased. The improvement in the fatigue strength of HVOF-coated specimens can be attributed to the fact that the compressive residual stress amplitude is higher when the coating thickness is increased. A clear trend of increasing magnitude of the compressive stress at the interface between the coating and the substrate as the coating thickness increases (see the inlet of Fig. 8) indicates the beneficial effect of increased coating thickness on the fatigue strength of HVOF-coated specimens.

Figure 15 shows the stress amplitude as a function of the number of cycles to failure of hard chrome-plated specimens with coating layer thicknesses of 30, 61, and 93 μm in the rotating bending fatigue tests. The values were averaged from three tests. The fatigue curves were fitted by the Basquin's equation. The fatigue strength of specimens with hard chrome coatings is lower than that of the substrate. A zoom in portion near the number of cycles of 10^7 is shown in the inlet of Fig. 15. The fatigue strength for the specimens plated with layer thicknesses of 30, 6, and 93 μm is 400, 390, and 370 MPa, respectively. Examination of the residual stress data shown in Fig. 9 revealed that the reduction in the fatigue strength of specimens with hard chrome coatings may be associated with the induced tensile residual stress in the plated layer. The hard chrome coatings exhibit tensile stress and microcracks. As the coating gets thicker, the microcrack density is greater and therefore the larger reduction in the fatigue strength. Dennis and Such (Ref 34) explained that the crack occurs in chromium coatings of steel substrates when the accumulated stress exceeds the tensile strength of chromium as the coating thickness increases. Almotairi et al. (Ref 35) plated chromium on steel substrates and found that residual stress and crack density in the chrome coatings increase with coating thickness. As shown in Fig. 7(d), (e) and (f), the microcrack density increases with coating thickness for the hard chrome-plated specimens. The microcracks density quantitative analysis indicated averaged values of 40 microcracks/mm, 57 microcracks/mm, and 67 microcracks/mm at the surface of the coated specimens with plating thicknesses of 30, 61, and 93 μm, respectively. It appeared that the density of microcracks, which increases with the plating thickness, might be a significant factor to influence the fatigue limit. Watanabe et al. (Ref 36) reported that the effect of coating thickness on the number of fatigue cracks appeared to be a sensitive parameter. It could be considered that the adhesion strength for the chrome-plated specimens

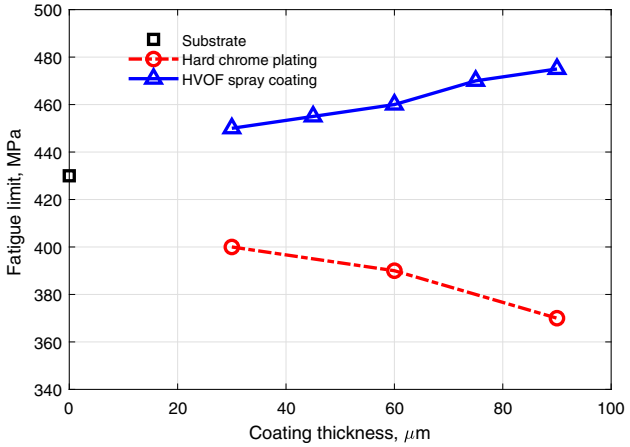

Fig. 16 The fatigue strength as a function of the coating thickness

decreased with increasing coating thickness. Nascimento et al. (Ref 37) also reported that microcracks form when the high tensile residual stresses exceed the cohesive strength of the chromium deposits and affect the fatigue behavior of a plated part. They also described that microcrack density arises as a relief of the tensile residual internal stresses, and the density increases when the chromium thickness increases.

Figure 16 shows a plot of the fatigue strength as a function of the coating thickness for the HVOF-coated specimens and the hard chrome-plated specimens. The fatigue strengths of HVOF-coated specimens are higher than those of the hard chrome-plated specimens at nearly the same coating thicknesses examined in this investigation. The specimens with HVOF WC-10Co-4Cr coatings have higher fatigue strengths than those without coatings. Rodríguez et al. (Ref 38) reported that proper surface finish and large compressive residual stress of the surface layer can increase the fatigue life of their AISI 1045 steel components. The HVOF WC-10Co-4Cr-coated specimens have higher fatigue strength than the hard chrome-plated specimens regardless of the higher surface roughness of the WC-10Co-4Cr coatings.

Conclusions

Effects of coating thickness on fatigue lives of HVOF WC-10Co-4Cr-coated and hard chrome-plated AISI 1045 steel shafts were investigated. Residual stresses of the coating layers were measured for the specimens with various thicknesses by an XRD technique. Magnitudes of the compressive residual stress increase as the distance from the substrate decreases for the HVOF-coated specimens with coating thicknesses of 31, 46, 63, 77, and 92 μm. The residual stresses in the hard chrome-plated coatings with thicknesses of 30, 61, and 93 μm are mostly tensile except the region near the interface between the coatings and the substrate. The fatigue strength of the HVOF-coated specimens tends to increase with the coating thickness. The increase in the fatigue strength can be attributed to the fact that the compressive residual stress at the interface between the coatings and the substrate increases as the coating thickness increases. In contrast, the fatigue strength of the hard chrome-plated specimens decreases when the coating thickness increases. Tensile residual stress and microcracks exist in the hard chrome coatings. As the coating thickness of chrome-plated specimens increases, the microcrack density gets higher and therefore the lower fatigue strength.

Acknowledgement The authors would like to express their appreciation to the staff of Ho Chi Minh City Center for Nuclear Techniques and the Metallurgy Laboratory at Ho Chi Minh City University of Technology and Education for their assistance. Helpful discussions with Dr. Huy Dong Pham of An Binh Coating Corporation are greatly appreciated.

References

1. D.T. Gawne, Failure of electrodeposited chromium coatings on cast iron substrates. Thin Solid Films **118**, 385–393 (1984)
2. J. Pina, A. Dias, M. Francois, J.L. Lebrun, Residual stresses and crystallographic texture in hard-chromium electroplated coatings. Surf. Coat. Technol. **96**, 148–162 (1997)
3. M.P. Nascimento, H.J.C. Voorwald, R.C. Souza, W.L. Pigatin, Evaluation of an electroless nickel interlayer on the fatigue and corrosion strength of chromium-plated AISI 4340 Steel. Plat. Surf. Finish. **88**, 84–90 (2001)
4. W. Pfeiffer, C. Koplin, E. Reisacher, J. Wenzel, Residual stresses and strength of hard chrome coatings. Mater. Sci. Forum **681**, 133–138 (2011)
5. A. Tipton, The effect of HVOF sprayed coatings on the elevated temperature high cycle fatigue behaviour of a martensitic stainless steel, In *Proceedings of the 8th National Thermal Spray Conference on Advances in Thermal Spray Science and Technology*. Houston/ASM International, Texas/Materials Park, 1995, p 463–468.
6. M.C. Nestler, G. Prenzel, and T. Seitz, HVOF-spraying v.s hard chrome plating coating characteristics and aircraft applications, in *Proceedings of the 15th International Thermal Spray Conference*, 1998, pp. 1073–1082
7. Y. Wu, B. Wang, S. Hong, J. Zhang, Y. Qin, G. Li, Dry sliding wear properties of HVOF sprayed WC-10Co-4Cr coating. Trans. Indian Inst. Met. **68**, 581–586 (2015)
8. A. Agüero, F. Camón, J. García de Blas, J.C. del Hoyo, R. Muelas, A. Santaballa, S. Ulargui, P. Vallé, HVOF-deposited WCCoCr as replacement for hard Cr in landing gear actuators. J. Therm. Spray Technol. **20**, 1292–1309 (2011)
9. M. Kutz, *Handbook of Environmental Degradation of Materials*, 2nd edn. (William Andrew Publishing, Sawston, 2012)
10. C.J. Villalobos-Gutiérrez, G.E. Gedler, J.G. La Barbera-Sosa, A. Piñeiro, M.H. Staia, J. Lesage, D. Chicot, G. Mesmacque, E.S. Puchi-Cabrera, Fatigue and corrosion fatigue behavior of an AA6063-T6 aluminum alloy coated with a WC-10Co-4Cr alloy deposited by HVOF thermal spraying. Surf. Coat. Technol. **202**, 4572–4577 (2008)

11. E.S. Puchi-Cabrera, M.H. Staia, M.J. Ortiz-Mancilla, J.G. La Barbera-Sosa, E.A. OchoaPérez, C. Villalobos-Gutiérrez, S. Bellayer, M. Traisnel, D. Chicot, J. Lesage, Fatigue Behavior of a SAE 1045 steel coated with colmonoy 88 alloy deposited by HVOF thermal spray. Surface Coat Technol. **205**, 1119–1126 (2010)
12. J.M. Azizpour, S. Nourouzi, Evaluation of surface residual stresses in HVOF sprayed WC-12Co coatings by XRD and ED-hole drilling. J. Mech. Sci. Technol. **27**, 2709–2713 (2013)
13. K.O. Legg, M. Graham, P. Chang, F. Rastagar, A. Gonzales, B. Sartwell, The replacement of electroplating. Surface Coat Technol. **81**, 99–105 (1996)
14. A. Ibrahim, C.C. Berndt, Fatigue and deformation of HVOF sprayed WC–Co coatings and hard chrome plating. Mater. Sci. Eng. A **456**, 114–119 (2007)
15. G. Silva-Junior, H.J.C. Voorwald, M.O.H. Cioffi, Evaluation of HVOF sprayed WC-13Co-4Cr and hard chrome electroplated on stainless steel 15–5PH fatigue strength, in *Proceedings of the 7th International Conference on Mechanics and Materials in Design Albufeira/Portugal*, 2017, p 11–15.
16. V.P. Nguyen, T.N. Dang, C.C. Le, Evaluating the effect of HVOF sprayed WC-10Co-4Cr and hard chromium electroplated coatings on fatigue strength of axle-shaped machine parts, in *Proceedings of the Internatioanl Conference on Engineering Research and Application. ICERA 2018. Lecture Notes in Networks and Systems*, vol 63. Springer, Cham, 2019, pp. 309–317.
17. H.J.C. Voorwald, R. Padilha, M.Y.P. Costa, W.L. Pigatin, M.O.H. Cioffi, Effect of electroless nickel interlayer on the fatigue strength of chromium electroplated AISI 4340 steel. Int. J. Fatigue **29**, 695–704 (2007)
18. C.C. Le, Development of automated X – ray stress analyzer and its applications in stress measurement of textured materials, in *Doctoral Thesis*, Nagaoka University of Technology, Japan, 2004.
19. J.M. Azizpour, H.M. Majd, Residual stress in ground WC-Co coatings. Int. J. Mater. Metal. Eng. **8**, 529–531 (2014)
20. B. Eigenmann, B. Scholtes, E. Macherauch, X-ray residual stress determination in thin chromium coatings on steel. Surf. Eng. **7**, 221–224 (1991)
21. H. Masoumi, S.M. Safavi, M. Salehi, S.M. Nahvi, Effect of grinding on the residual stress and adhesion strength of HVOF thermally sprayed WC-10Co-4Cr Coating. Mater. Manuf. Processes **29**, 1139–1151 (2014)
22. J.M. Azizpour, S. Norouzi, H.M. Majd, Mechanical properties of WC-12Co HVOF coatings. J. Am. Sci. **7**, 609–614 (2011)
23. H.J.C. Voorwald, R.C. Souza, W.L. Pigatin, M.O.H. Cioffi, Evaluation of WC–17Co and WC-10Co-4Cr thermal spray coatings by HVOF on the fatigue and corrosion strength of AISI 4340 steel. Surf. Coat. Technol. **190**, 155–164 (2005)
24. C. Lyphout, P. Nyle´n, A. Manescu, TPirling, Residual stresses distribution through thick HVOF sprayed inconel 718 coatings. J. Therm. Spray Technol. **17**, 915–923 (2008)
25. A. Valarezo, G. Bolelli, W.B. Choi, S. Sampath, V. Cannillo, L. Lusvarghi, R. Rosa, Damage tolerant functionally graded WC-Co/stainless steel HVOF coatings. Surf. Coat. Technol. **205**(7), 2197–2208 (2010)
26. S. Kuroda, Y. Tashiro, H. Yumoto, S. Taira, H. Fukanuma, S. Tobe, peening action and residual stresses in high velocity oxygen fuel thermal spraying of 316L stainless steel. J. Therm. Spray Technol. **10**(2), 367–374 (2001)
27. S. Sampath, X.Y. Jiang, J. Matejicek, L. Prchlik, A. Kulkarni, A. Vaidya, Role of thermal spray processing method on the microstructure, residual stress and properties of coatings: an integrated study for Ni–5 wt.%Al bond coats. Mater. Sci. Eng. A **364**, 216–231 (2004)
28. P. Bansal, P.H. Shipway, S.B. Leen, Effect of particle impact on residual stress development in HVOF sprayed coatings. J. Therm. Spray Technol. **15**(4), 570–575 (2006)
29. M. Gui, R. Eybel, B. Asselin, S. Radhakrishnan, J. Cerps, Influence of processing parameters on residual stress of high velocity Oxy-Fuel thermally sprayed WC-Co-Cr coating. J. Mater. Eng. Perform. **21**(10), 2090–2098 (2012)
30. M. Ohtsuka, H. Matsuoka, Y. Hirose, H. Ishii, Young's modulus measurement of chromium electroplating. Adv. X-Ray Anal. **35**, 527–535 (1991)
31. M.Y.P. Costa, M.L.R. Venditti, H.J.C. Voorwald, M.O.H. Cioffi, T.G. Cruz, Effect of WC-10%Co-4%Cr coating on the Ti-6Al-4V alloy fatigue strength. Mater. Sci. Eng. A **507**(1–2), 29–36 (2009)
32. M.P. Nascimento, R.C. Souza, W.L. Pigatin, H.J.C. Voorwald, Effects of surface treatments on the fatigue strength of AISI 4340 aeronautical steel. Int. J. Fatigue **23**(7), 607–618 (2001)
33. O.H. Basquin, The exponential law of endurance test, ASTM STP, 1910, 10, p 625–630
34. J.K. Dennis, T.E. Such, *Nickel and chromium plating*, 3rd edn. (Woodheah Publishing Ltd., Sawston, 1993), p. 218
35. A. Almotairi, A. Warkentin, Z. Farhat, Mechanical damage of hard chrome coatings on 416 stainless steel. Eng. Fail. Anal. **66**, 130–140 (2016)
36. S. Watanabe, T. Tajiri, N. Sakoda, J. Amano, Fatigue cracks in HVOF thermally sprayed WC-Co coatings. J. Therm. Spray Technol. **7**(1), 93–96 (1998)
37. M.P. Nascimento, R.C. Souza, I.M. Miguel, W.L. Pigatin, H.J.C. Voorwald, Effects of tungsten carbide thermal spray coating by HP/HVOF and hard chromium electroplating on AISI 4340 high strength steel. Surf. Coat. Technol. **138**(2–3), 113–124 (2001)
38. A. Rodríguez, L.N. López de Lacalle, A. Celaya, A. Lamikiz, J. Albizuri, Surface improvement of shafts by the deep ball-burnishing technique. Surf. Coat. Technol. **206**, 2817–2824 (2012)